

ESI for “Bayesian determination of the effect of a deep eutectic solvent on the structure of lipid monolayers”

Andrew R. McCluskey,^{ab‡} Adrian Sanchez-Fernandez,^{ac‡¶}
Karen J. Edler,^{a*} Stephen C. Parker,^a Andrew J. Jackson,^{cd}
Richard A. Campbell,^{ef} and Thomas Arnold^{abcg*}

^a Department of Chemistry, University of Bath, Claverton Down, Bath, BA2 7AY, UK.

^b Diamond Light Source, Harwell Campus, Didcot, OX11 0DE, UK.

^c European Spallation Source, SE-211 00 Lund, Sweden.

^d Department of Physical Chemistry, Lund University, SE-211 00 Lund, Sweden.

^e Institut Laue-Langevin, 71 avenue des Martyrs, 38000, Grenoble, France.

^f Division of Pharmacy and Optometry, University of Manchester, Manchester, M13 9PT, UK.

^g ISIS Neutron and Muon Source, Science and Technology Facilities Council, Rutherford Appleton Laboratory, Harwell Oxford, Didcot OX11 0QX, UK.

¶ Present address: Department of Food Technology, Lund University, SE-211 00 Lund, Sweden

1 Grazing incident X-ray diffraction (GIXD)

GIXD was measured for DPPC and DMPC at 30 mN m^{-1} at 22°C (and 7°C for DMPC), and are shown in Figures 1-3. All figures contain an artifact from the X-ray beam interacting with the Teflon of the Langmuir trough. However, in figures 1 and 3 it is possible to identify a (2, 0) diffraction peak that indicates the presence of a similar structure to that found under the same conditions in water.¹ Based on this information we believe that, similar to water, the phase of the lipid tails is likely to be in the liquid phase at all surface pressures measured.

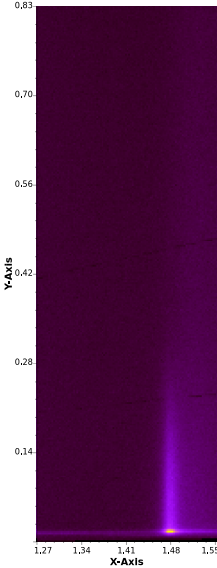


Figure 1: The GIXD pattern for DPPC at 30 mN m^{-1} at 22°C , the axes at in units of \AA^{-1} . Source: Datasets, figure files and running/plotting scripts are available under CC-BY.²

2 XRR parameters at each surface pressure

3 Probability distribution functions

The two-dimensional probability distribution functions (PDFs) for all parameters and all lipids from the X-ray reflectometry models are given in Figures 4-19. The two-dimensional probability distribution functions (PDFs) for all parameters and all lipids from the neutron reflectometry models are given in Figures 20-23.

References

- [1] E. B. Watkins, C. E. Miller, D. J. Mulder, T. L. Kuhl, and J. Majewski, *Phys. Rev. Lett.*, 2009, **102**, 238101.
- [2] A. R. McCluskey, *XRR, and SLD profiles, head volume PDFs and tail thickness and solvent fraction. Data, figures and plotting script on figshare*, 2018, <https://doi.org/10.6084/m9.figshare.7053410>.

Table 1: The best-fit values, and associated 95 % confidence intervals for the varying parameters in the XRR models, at the second highest surface pressure (SP) measured. The values of d_t were found from the values of θ_t using Eqn. ?? and the values for ϕ_h were obtained from the use of Eqn. ??

Lipid	DLPC	DMPC	DPPC	DMPG
SP/mNm ⁻¹	30	30	25	25
$\theta_t/^\circ$	$51.99^{+0.18}_{-0.18}$	$40.28^{+0.06}_{-0.06}$	$34.89^{+0.07}_{-0.06}$	$47.12^{+0.05}_{-0.05}$
$\sigma_{t,h,s}/\text{\AA}$	$4.17^{+0.02}_{-0.02}$	$3.86^{+0.00}_{-0.00}$	$4.31^{+0.00}_{-0.00}$	$3.81^{+0.00}_{-0.00}$
$V_t/\text{\AA}^3$	$625.18^{+3.61}_{-3.87}$	$718.76^{+0.53}_{-0.52}$	$765.31^{+0.39}_{-0.37}$	$734.01^{+0.59}_{-0.58}$
$V_h/\text{\AA}^3$	$331.43^{+0.62}_{-0.62}$	$339.55^{+0.27}_{-0.27}$	$322.00^{+0.24}_{-0.25}$	$329.95^{+0.36}_{-0.33}$
$d_h/\text{\AA}$	$10.95^{+0.14}_{-0.29}$	$13.21^{+0.04}_{-0.04}$	$12.69^{+0.03}_{-0.03}$	$13.95^{+0.03}_{-0.03}$
$\phi_h/\times 10^{-2}$	$54.11^{+1.06}_{-1.07}$	$50.93^{+0.23}_{-0.23}$	$44.24^{+0.23}_{-0.22}$	$60.57^{+0.17}_{-0.17}$
$d_t/\text{\AA}$	$9.52^{+0.04}_{-0.04}$	$13.72^{+0.01}_{-0.01}$	$16.83^{+0.01}_{-0.01}$	$12.24^{+0.01}_{-0.01}$

Table 2: The best-fit values, and associated 95 % confidence intervals for the varying parameters in the XRR models, at the second lowest surface pressure (SP) measured. The values of d_t were found from the values of θ_t using Eqn. ?? and the values for ϕ_h were obtained from the use of Eqn. ??

Lipid	DLPC	DMPC	DPPC	DMPG
SP/mNm ⁻¹	25	25	20	20
$\theta_t/^\circ$	$57.54^{+0.17}_{-0.17}$	$47.63^{+0.05}_{-0.05}$	$36.11^{+0.06}_{-0.06}$	$53.73^{+0.04}_{-0.04}$
$\sigma_{t,h,s}/\text{\AA}$	$4.36^{+0.02}_{-0.02}$	$3.92^{+0.01}_{-0.01}$	$4.09^{+0.00}_{-0.00}$	$3.95^{+0.01}_{-0.01}$
$V_t/\text{\AA}^3$	$625.18^{+3.61}_{-3.87}$	$718.76^{+0.53}_{-0.52}$	$765.31^{+0.39}_{-0.37}$	$734.01^{+0.59}_{-0.58}$
$V_h/\text{\AA}^3$	$331.43^{+0.62}_{-0.62}$	$339.55^{+0.27}_{-0.27}$	$322.00^{+0.24}_{-0.25}$	$329.95^{+0.36}_{-0.33}$
$d_h/\text{\AA}$	$10.95^{+0.14}_{-0.29}$	$13.21^{+0.04}_{-0.04}$	$12.69^{+0.03}_{-0.03}$	$13.95^{+0.03}_{-0.03}$
$\phi_h/\times 10^{-2}$	$60.00^{+0.94}_{-0.93}$	$56.66^{+0.21}_{-0.20}$	$45.08^{+0.22}_{-0.21}$	$65.72^{+0.14}_{-0.15}$
$d_t/\text{\AA}$	$8.30^{+0.04}_{-0.04}$	$12.12^{+0.01}_{-0.01}$	$16.57^{+0.01}_{-0.01}$	$10.64^{+0.01}_{-0.01}$

Table 3: The best-fit values, and associated 95 % confidence intervals for the varying parameters in the XRR models, at the lowest surface pressure (SP) measured. The values of d_t were found from the values of θ_t using Eqn. ?? and the values for ϕ_h were obtained from the use of Eqn. ??

Lipid	DLPC	DMPC	DPPC	DMPG
SP/mNm ⁻¹	20	20	15	15
$\theta_t/^\circ$	$63.26^{+0.12}_{-0.12}$	$58.51^{+0.04}_{-0.04}$	$38.97^{+0.06}_{-0.06}$	$71.51^{+0.18}_{-0.18}$
$\sigma_{t,h,s}/\text{\AA}$	$4.23^{+0.02}_{-0.02}$	$4.20^{+0.01}_{-0.01}$	$3.88^{+0.00}_{-0.00}$	$4.65^{+0.01}_{-0.01}$
$V_t/\text{\AA}^3$	$625.18^{+3.61}_{-3.87}$	$718.76^{+0.53}_{-0.52}$	$765.31^{+0.39}_{-0.37}$	$734.01^{+0.59}_{-0.58}$
$V_h/\text{\AA}^3$	$331.43^{+0.62}_{-0.62}$	$339.55^{+0.27}_{-0.27}$	$322.00^{+0.24}_{-0.25}$	$329.95^{+0.36}_{-0.33}$
$d_h/\text{\AA}$	$10.95^{+0.14}_{-0.29}$	$13.21^{+0.04}_{-0.04}$	$12.69^{+0.03}_{-0.03}$	$13.95^{+0.03}_{-0.03}$
$\phi_h/\times 10^{-2}$	$66.47^{+0.74}_{-0.75}$	$66.41^{+0.16}_{-0.16}$	$47.15^{+0.22}_{-0.21}$	$81.62^{+0.18}_{-0.18}$
$d_t/\text{\AA}$	$6.95^{+0.03}_{-0.03}$	$9.39^{+0.01}_{-0.01}$	$15.95^{+0.01}_{-0.01}$	$5.70^{+0.05}_{-0.05}$

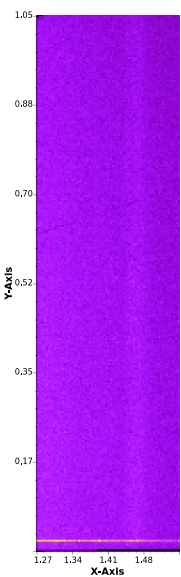


Figure 2: The GIXD pattern for DMPC at 30 mN m^{-1} at 22°C , the axes at in units of \AA^{-1} . Source: Datasets, figure files and running/plotting scripts are available under CC-BY.²

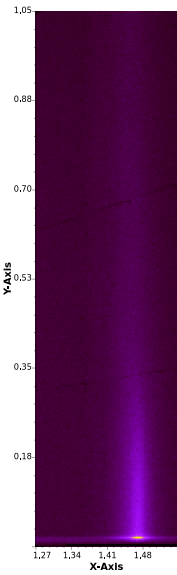


Figure 3: The GIXD pattern for DMPC at 30 mN m^{-1} at 7°C , the axes at in units of \AA^{-1} . Source: Datasets, figure files and running/plotting scripts are available under CC-BY.²

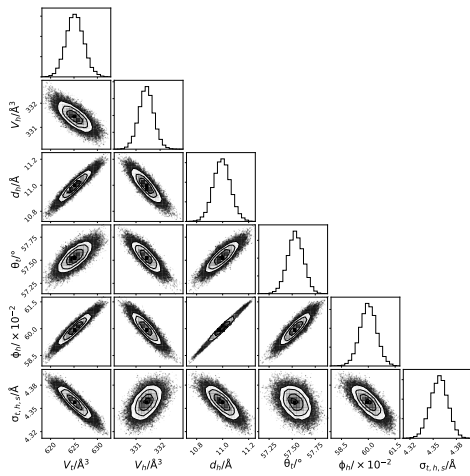


Figure 4: The multi-parameter PDFs for the chemically-relevant model of DLPC X-ray reflectometry data at 20 mNm^{-1} . Source: Datasets, figure files and running/plotting scripts are available under CC-BY.²

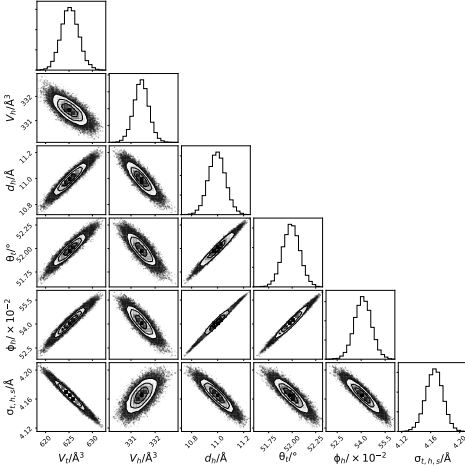


Figure 5: The multi-parameter PDFs for the chemically-relevant model of DLPC X-ray reflectometry data at 25 mNm^{-1} . Source: Datasets, figure files and running/plotting scripts are available under CC-BY.²

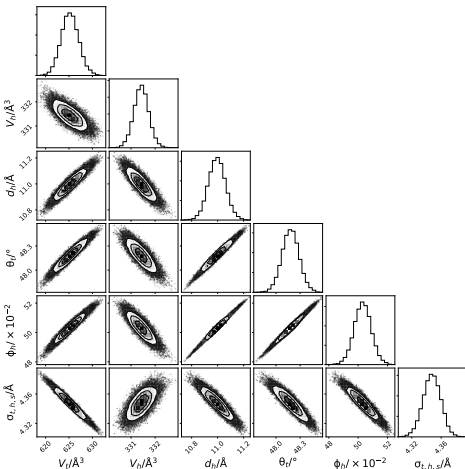


Figure 6: The multi-parameter PDFs for the chemically-relevant model of DLPC X-ray reflectometry data at 30 mNm^{-1} . Source: Datasets, figure files and running/plotting scripts are available under CC-BY.²

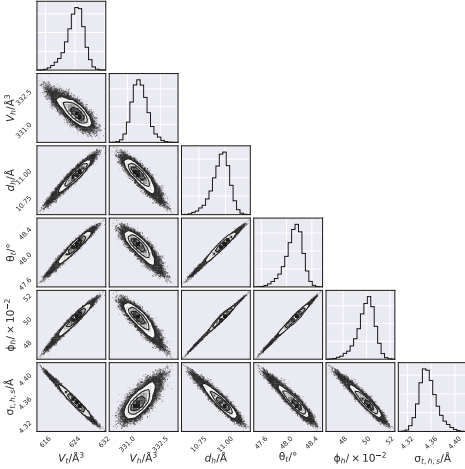


Figure 7: The multi-parameter PDFs for the chemically-relevant model of DLPC X-ray reflectometry data at 35 mNm^{-1} . Source: Datasets, figure files and running/plotting scripts are available under CC-BY.²

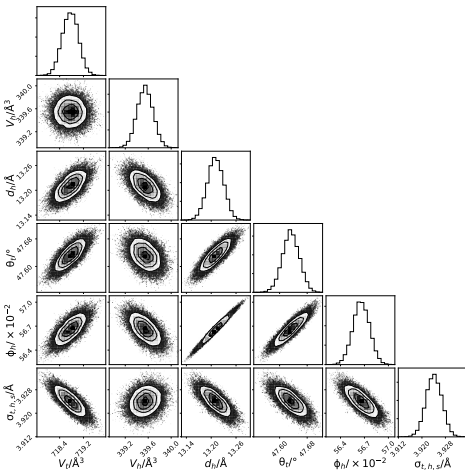


Figure 8: The multi-parameter PDFs for the chemically-relevant model of DMPC X-ray reflectometry data at 20 mNm^{-1} . Source: Datasets, figure files and running/plotting scripts are available under CC-BY.²

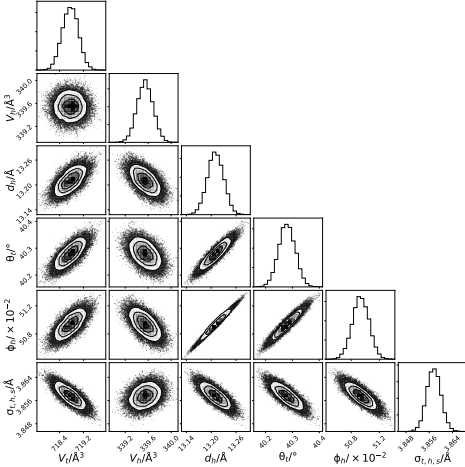


Figure 9: The multi-parameter PDFs for the chemically-relevant model of DMPC X-ray reflectometry data at 25 mNm^{-1} . Source: Datasets, figure files and running/plotting scripts are available under CC-BY.²

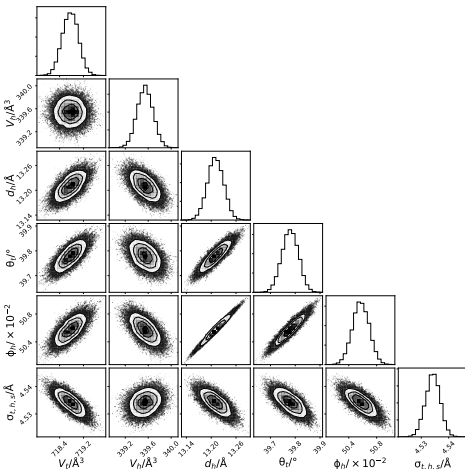


Figure 10: The multi-parameter PDFs for the chemically-relevant model of DMPC X-ray reflectometry data at 30 mNm^{-1} . Source: Datasets, figure files and running/plotting scripts are available under CC-BY.²

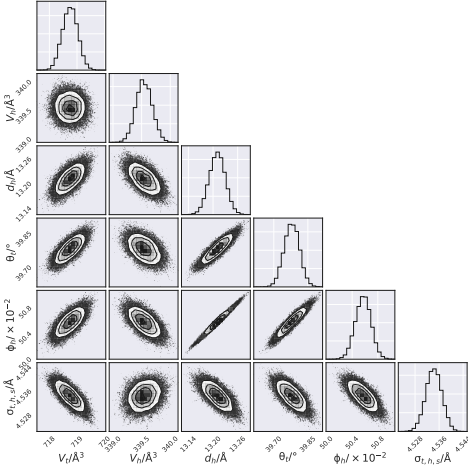


Figure 11: The multi-parameter PDFs for the chemically-relevant model of DMPC X-ray reflectometry data at 40 mNm^{-1} . Source: Datasets, figure files and running/plotting scripts are available under CC-BY.²

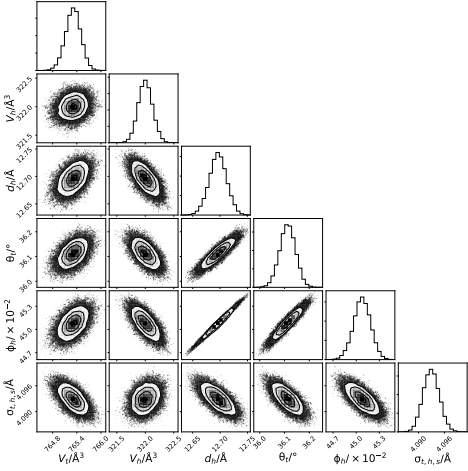


Figure 12: The multi-parameter PDFs for the chemically-relevant model of DPPC X-ray reflectometry data at 15 mNm^{-1} . Source: Datasets, figure files and running/plotting scripts are available under CC-BY.²

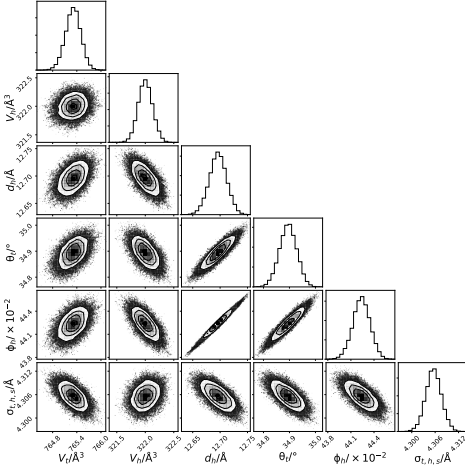


Figure 13: The multi-parameter PDFs for the chemically-relevant model of DPPC X-ray reflectometry data at 20 mNm^{-1} . Source: Datasets, figure files and running/plotting scripts are available under CC-BY.²

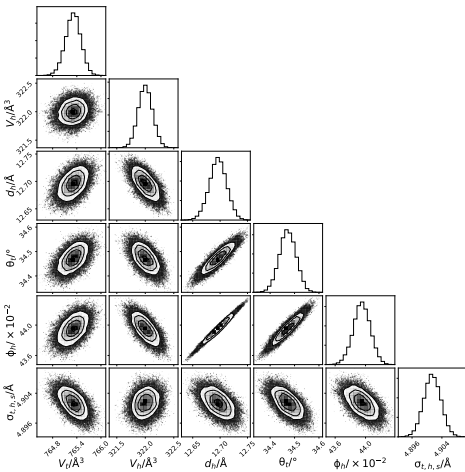


Figure 14: The multi-parameter PDFs for the chemically-relevant model of DPPC X-ray reflectometry data at 25 mNm^{-1} . Source: Datasets, figure files and running/plotting scripts are available under CC-BY.²

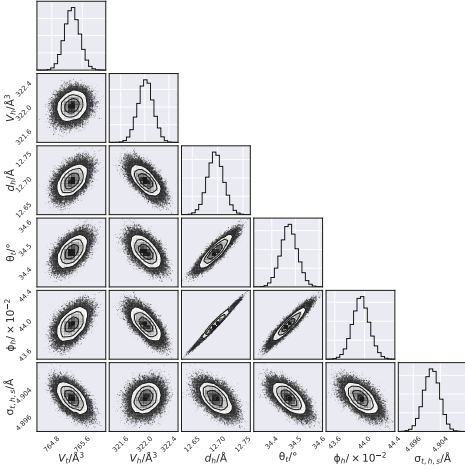


Figure 15: The multi-parameter PDFs for the chemically-relevant model of DPPC X-ray reflectometry data at 30 mNm⁻¹. Source: Datasets, figure files and running/plotting scripts are available under CC-BY.²

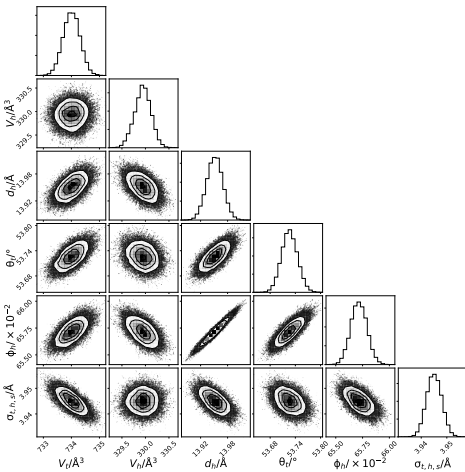


Figure 16: The multi-parameter PDFs for the chemically-relevant model of DMPG X-ray reflectometry data at 15 mNm⁻¹. Source: Datasets, figure files and running/plotting scripts are available under CC-BY.²

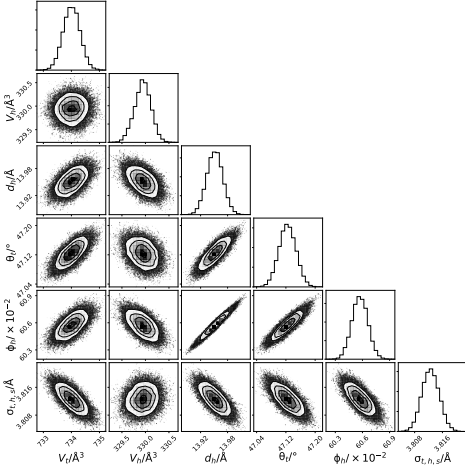


Figure 17: The multi-parameter PDFs for the chemically-relevant model of DMPG X-ray reflectometry data at 20 mNm^{-1} . Source: Datasets, figure files and running/plotting scripts are available under CC-BY.²

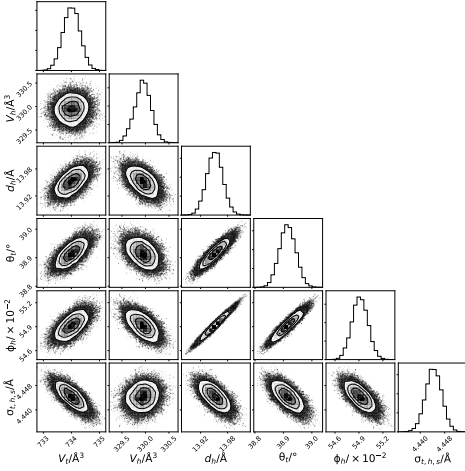


Figure 18: The multi-parameter PDFs for the chemically-relevant model of DMPG X-ray reflectometry data at 25 mNm^{-1} . Source: Datasets, figure files and running/plotting scripts are available under CC-BY.²

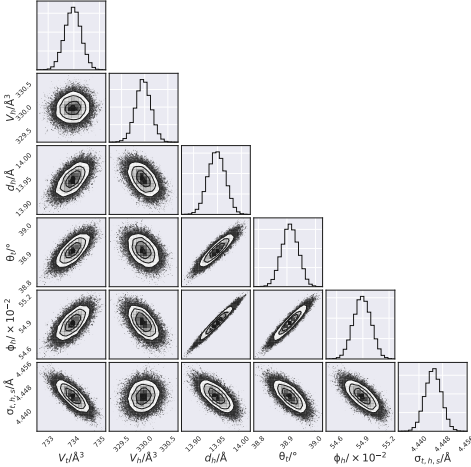


Figure 19: The multi-parameter PDFs for the chemically-relevant model of DMPG X-ray reflectometry data at 30 mNm^{-1} . Source: Datasets, figure files and running/plotting scripts are available under CC-BY.²

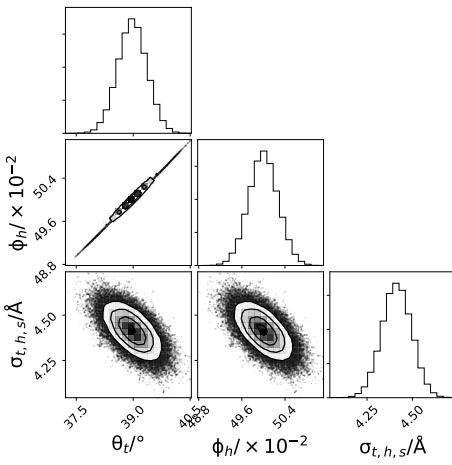


Figure 20: The multi-parameter PDFs for the chemically-relevant model of two contrast DMPC neutron reflectometry data at 20 mNm^{-1} . Source: Datasets, figure files and running/plotting scripts are available under CC-BY.²

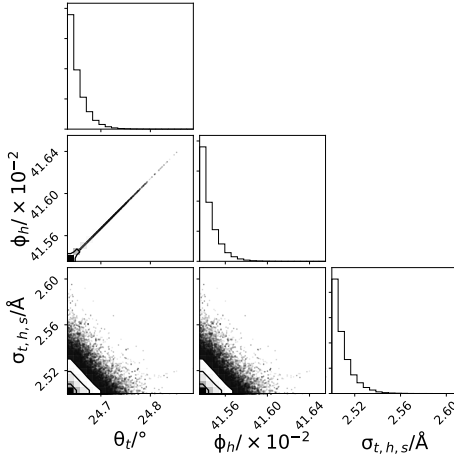


Figure 21: The multi-parameter PDFs for the chemically-relevant model of two contrast DMPC neutron reflectometry data at 25 mNm^{-1} . Source: Datasets, figure files and running/plotting scripts are available under CC-BY.²

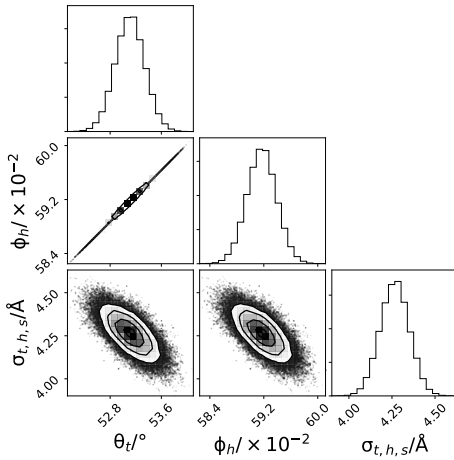


Figure 22: The multi-parameter PDFs for the chemically-relevant model of two contrast DPPC neutron reflectometry data at 15 mNm^{-1} . Source: Datasets, figure files and running/plotting scripts are available under CC-BY.²

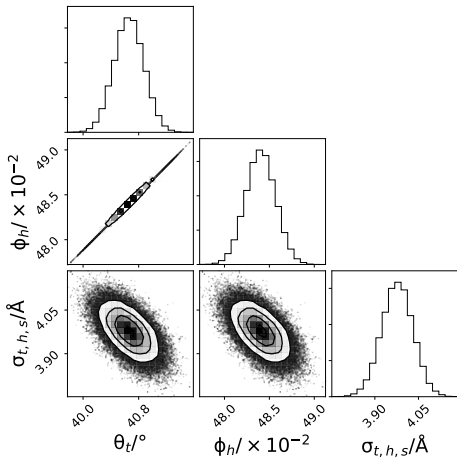


Figure 23: The multi-parameter PDFs for the chemically-relevant model of two contrast DMPC neutron reflectometry data at 20 mNm^{-1} . Source: Datasets, figure files and running/plotting scripts are available under CC-BY.²